A Journal of the Gesellschaft Deutscher Chemiker

Angewandte International Edition GDCh Chemie

www.angewandte.org

Accepted Article

Title: Capture and Separation of SO2 Traces in Metal-Organic Frameworks via Pre-synthetic Pore Environment Tailoring by Methyl Groups

Authors: Shanghua Xing, Jun Liang, Philipp Brandt, Felix Schäfer, Alexander Nuhnen, Tobias Heinen, Istvan Boldog, Jens Möllmer, Marcus Lange, Oliver Weingart, and Christoph Janiak

To be cited as: *Angew. Chem. Int. Ed.* 10.1002/anie.202105229

Link to VoR: https://doi.org/10.1002/anie.202105229

WILEY-VCH

10.1002/anie.202105229

WILEY-VCH

RESEARCH ARTICLE

Capture and Separation of SO_2 Traces in Metal-Organic Frameworks via Pre-synthetic Pore Environment Tailoring by Methyl Groups

Shanghua Xing,[a,b] Jun Liang,[a,b] Philipp Brandt,[b] Felix Schäfer,[c] Alexander Nuhnen,[b] Tobias Heinen,[b] Istvan Boldog,[b] Jens Möllmer,[d] Marcus Lange,[d] Oliver Weingart,*[c] and Christoph Janiak*[a,b]

[a] Dr. S. H. Xing, Dr. J. Liang, Prof. Dr. C. Janiak
Hoffmann Institute of Advanced Materials,
Shenzhen Polytechnic
7098 Liuxian Blvd, Nanshan District, Shenzhen 518055, China
E-mail: janiak@hhu.de

[b] Dr. S. H. Xing, Dr. J. Liang, P. Brandt, Dr. A. Nuhnen, T. Heinen, Dr. I. Boldog, Prof. Dr. C. Janiak
Institut für Anorganische Chemie und Strukturchemie,
Heinrich-Heine-Universität Düsseldorf
40225 Düsseldorf, Germany

[c] F. Schäfer, Dr. O. Weingart
Institut für Theoretische Chemie und Computerchemie,
Heinrich-Heine-Universität Düsseldorf
40225 Düsseldorf, Germany
E-mail: oliver.weingart@hhu.de

[d] Dr. J. Möllmer, Dr. M. Lange
Institut für Nichtklassische Chemie e.V.
Permoserstraße 15, 04318 Leipzig, Germany

Supporting information for this article is given via a link at the end of the document.

Abstract: Herein, we report a pre-synthetic pore environment design strategy to achieve stable methyl-functionalized metal-organic frameworks (MOFs) for preferential SO_2 binding and thus enhanced low (partial) pressure SO_2 adsorption and SO_2/CO_2 separation. The enhanced sorption performance is for the first time attributed to an optimal pore size by increasing methyl group densities at the benzenedicarboxylate linker in $[Ni_2(BDC\text{-}X)_2DABCO]$ (BDC-X = mono-, di- and tetramethyl-1,4-benzenedicarboxylate/terephthalate; DABCO = 1,4-diazabicyclo[2,2,2]octane). Monte Carlo simulations and first-principles density-functional theory (DFT) calculations demonstrate the key role of methyl groups within the pore surface on the preferential SO_2 affinity over the parent MOF. The SO_2 separation potential by methyl-functionalized MOFs has been validated by gas sorption isotherms, ideal adsorbed solution theory calculations, simulated breakthrough curves and DFT calculations.

Introduction

The emission of the toxic gas sulfur dioxide (SO_2) represents one of the most serious pollutions and continues to threaten human health and pose various environment issues.[1,2,3,4] Although a large fraction (~95%) of SO_2 is removed from flue gases by established desulfurization technologies such as limestone scrubbing,[1,5] the residual SO_2 still remains in flue gas and can damage other gas scrubbers.[6,7] Developing new technologies based on solid adsorbents for trace SO_2 removal could be a possibility in view of process economy and energy-efficiency.[8,9,10,11] Given the highly corrosive nature of SO_2, many materials are sensitive to SO_2 and thus relatively limited studies have been performed on ionic liquids,[12] zeolite,[13] porous organic cages[14] and metal-organic frameworks (MOFs). [15,16,17,18,19,20,21] Among them, MOFs seem most promising due to their outstanding features including reticular synthesis, tunable structure and high porosity.[22,23,24,25] Up to now, there is still a small number of MOFs reported for SO_2 adsorption,[26,27,28] when compared to CO_2 and CH_4 sorption. Less effort was even given to targeted *trace* SO_2 removal, that is, high SO_2 uptake at low partial pressure. In general, the capacity of trace SO_2 removal is quantified by SO_2 uptake amount at a partial pressure of 0.1 bar or even 0.01 bar. So far, two main strategies for the enhanced SO_2 affinity have been proposed on MOFs. One is open metal sites within MOFs structure for M-SO_2 interactions.[29,30] The other one is polar amino groups in the framework as sites for hydrogen-bonding interactions to SO_2.[31,32] In addition, it has been recently

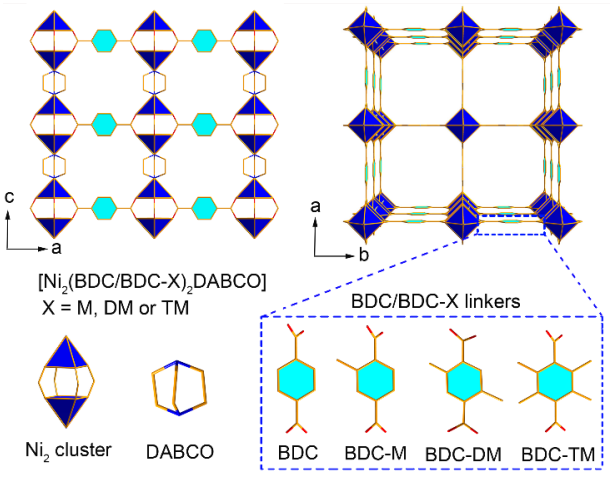

Figure 1. Top row: Sections of the packing diagram of DMOF showing the channel structures along the b- (and identical a-) axis and along the c-axis. Bottom row: The building blocks of the Ni_2 cluster, DABCO and BDC/BDC-X in DMOF/DMOF-X. X represent the monomethyl (M), 2,5 dimethyl (DM) or 2,3,5,6 tetramethyl (TM) substituents. Hydrogen atoms are omitted for clarity.

pointed out that small micropore diameters in the range of ~4 to 8 Å could be advantageous for low-pressure SO_2 uptake.[33]

MOFs with methyl-"functionalized" linkers could be a good candidate to tailor micropore diameters to the optimal range and at the same time have moderate non-covalent van der Waals interactions to SO_2 molecules for sufficient SO_2 affinity but still facile regeneration. Methyl-"functionalized" MOFs have been shown to display enhanced CO_2 uptake affinity,[34,35] but were not explored for SO_2 sorption and separation to the best of our knowledge. We propose that MOFs with an already feasible topology could be tuned in their pore diameter for an efficient SO_2 separation through methyl-"functionalization". At the same time, methyl groups increase the hydrophobicity and can shield the reactive metal-linker bonds to increase the stability of MOFs towards moisture.[25,36]

To the best of our knowledge, there is no work on the use of methyl groups to increase SO_2 affinity and SO_2/CO_2 selectivity. Herein, we systematically study the methyl-"functionalized" BDC linker in pillar-layered $[Ni_2(BDC\text{-}X)_2DABCO]$ {BDC-X = monomethyl (X = M), 2,5-dimethyl (X = DM) and tetramethyl (X = TM) 1,4-benzenedicarboxylate/terephthalate; DABCO = 1,4-diazabicyclo[2,2,2]octane} referred as DMOF-X (Figure 1).[37,38] DMOFs with different metals and linkers, mixed-metals and mixed-linkers, including BDC-TM and Ni-DMOF-TM were recently tested for SO_2 sorption with the focus on stability in humid conditions.[25] The addition of methyl groups to the BDC linker yields isostructural DMOFs.[39] The increased density of methyl groups in methyl-"functionalized" DMOF-X (X represent M, DM and TM) is then correlated to the SO_2 adsorption and separation properties.

Results and Discussion

The pillar-layered $[Ni_2(BDC)_2DABCO]$ DMOF is composed of dinuclear nickel paddlewheel units, $\{Ni_2(OOC\text{-})_4\}$ bridged by BDC linkers to form 2D regular square layers, which are further pillared by DABCO linkers to result in a 3D framework (Figure 1). Thus, two kinds of channels exist in this DMOF structure. One is the wide square channel with ~7.5 × 7.5 $Å^2$ along the c-axis (Figure 1, top-right), while the other is a more narrow rectangular aperture with ~5.6 × 6.9 $Å^2$ along the a- and b-axis (Figure 1, top-left).[37] The introduction of four methyl groups with the tetramethyl-terephthalate linker minimizes the pore width range of DMOF from ~6-8 Å down to ~5-7 Å in DMOF-TM (as determined from Ar sorption, Figure S11, SI). This agrees with the pore widths along the *c*-axis and *a*/*b*-axis in the DMOF-TM crystal structure of ~4.9 × 4.9 $Å^2$ and ~4.5 × 6.7 $Å^2$ respectively.[39] In BDC-TM, the tetramethylphenyl group also rotates out of the plane of the carboxylate groups, due to the steric effect of the methyl groups (Figure S1 and S2, SI).

The PXRD patterns of methyl-functionalized DMOF-X match with that of the parent DMOF, indicating their isostructural frameworks (Figure S3, SI). The solution ^1H NMR spectra (Figure S5-S8, SI) of digested DMOF and methyl-functionalized DMOF-X confirmed the expected 2:1 molar ratio of BDC/BDC-X to DABCO linker according to the formular of $[Ni_2(BDC/BDC\text{-}X)_2DABCO]$, being consistent with the results from elemental analysis (see Section S3, SI). Compared to DMOF, a trend of gradually reduced particle size with increased methylation to DMOF-TM was observed from SEM analysis (Figure S9, SI), attributed to a relative to each other increased nucleation and reduced growth rate with the increased number of methyl groups. From N_2 and Ar sorption isotherms at 77 and 87 K (Figure S11 and S12, SI), respectively, the Brunauer–Emmett–Teller (BET) surface area and pore volume of DMOF and DMOF-X decreased with the increasing number of methyl groups (Table 1), which fill the pores and limit the accessible surface area.

The SO_2 sorption isotherm of DMOF shows a slight S-shape (relatively low SO_2 affinity, see below) with the steep uptake setting in at 0.04 bar (Figure 2b). The SO_2 uptake of DMOF-X at 293 K sets in at decreasingly lower pressure (Figure 2b) with increasing number of methyl groups. At 0.01 bar, the SO_2 uptake of DMOF was recorded as 0.25 mmol·g^{-1}, while DMOF-M, DMOF-DM and DMOF-TM showed already an increased uptake of 0.46, 1.00 and 3.79 mmol·g^{-1} (Table 1, Figure 2b). Particularly, the SO_2 uptake of DMOF-TM (3.79 mmol·g^{-1}) at 0.01 bar exceeds most of the current top-performing MOFs (Figure S13 and Table S4, SI), such as Mg-MOF-74 (3.03 mmol·g^{-1}), SIFSIX-1-Cu (3.43 mmol·g^{-1}), SIFSIX-3-M (2.43 and 1.68 mmol·g^{-1} for M = Ni and Zn,

Table 1. Porosity characteristics of DMOF and DMOF-X and the results of SO_2 adsorption at 293 K.

Material	BET-surface area[a] (from N_2/Ar) [m^2 g^{-1}]	Total pore volume[b] (from N_2/Ar) [cm^3 g^{-1}]	Pore width[c] [Å]	SO_2-uptake (293 K) [mmol·g^{-1}] at			SO_2/CO_2 selectivity [d] at SO_2/CO_2 molar ratio		
				0.01 bar	0.1 bar	0.97 bar	0.01	0.1	0.5
DMOF Lit.[37]	2050[39]/–	0.80[39]/–	7.5, 5.6×6.9[37, e]	–	–	9.97 (298)[17]	–	–	–
DMOF	1956/1843	0.76/0.67	~6-8	0.25	7.21	13.09	18	36	92
DMOF-M	1557/1586	0.63/0.59	~6-8	0.46	6.40	12.15	27	38	81
DMOF-DM	1343/1281	0.52/0.56	~6-8	1.00	5.70	10.40	50	40	31
DMOF-TM	900/1079	0.43/0.42	~5-7	3.79	6.43	9.68	134	169	253
DMOF-TM Lit.[39]	894[39]/–	0.39[39]/–	4.5.[39, e]	–	–	~4.9 (298)[25]	–	–	–

[a] Obtained from five adsorption points in the pressure range $0.001 < p{\cdot}p_0^{-1} < 0.05$. [b] Derived at $p\ p_0^{-1} = 0.9$. [c] Pore widths from pore size distribution are measured by Ar sorption at 87 K. [d] See Section 5.2 in the SI for the CO_2 sorption data. [e] From X-ray structure.

10.1002/anie.202105229

respectively) and NH_2-MIL-125(Ti) (3.0 mmol·g^{-1}), and is only slightly lower than SIFSIX-2-Cu-i (4.16 mmol·g^{-1})[31,40] and MIL-160 (4.2 mmol·g^{-1}).[31] The latter two feature polar groups (SiF_6^{2-} and a furan ring, respectively) together with optimal micropore widths of ~5 Å (see below). As the pressure increased to 0.1 bar, SO_2 uptake of DMOF-TM rapidly rose up to 6.43 mmol·g^{-1} accounting for ~66% of the SO_2 uptake (9.68 mmol·g^{-1} at 0.97 bar). The observed high SO_2 uptake of DMOF- TM at low pressure (< 0.1 bar) meets a prerequisite of potential adsorptive flue-gas desulfurization processes. The SO_2 uptake at ~1 bar shows a reasonable linear relation relative to the BET surface area and pore volume (Figure 3). The SO_2 capacity at 0.97 bar was rationally decreased with increasing density of methyl groups on DMOF, which can be attributed to the gradually decreased pore volume and BET surface area (Table 1 and Figure 3).

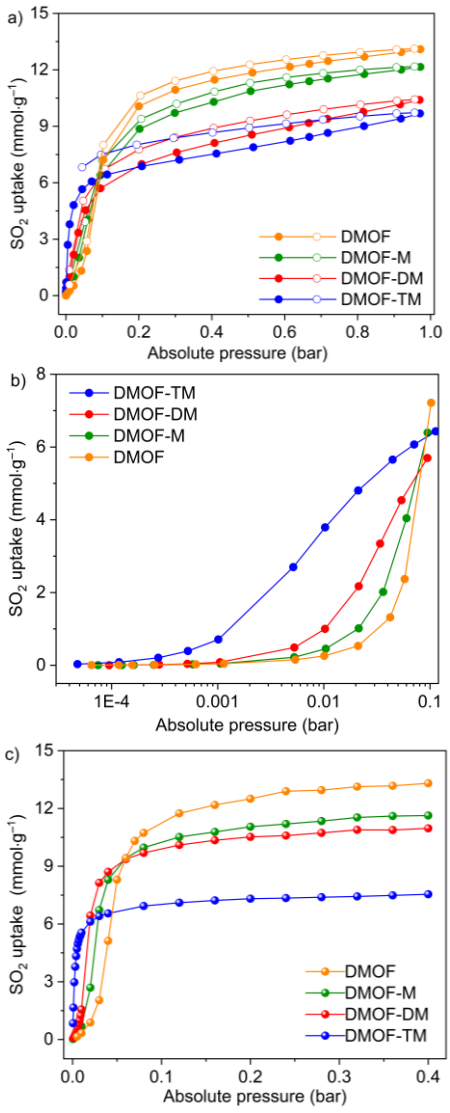

Figure 2. (a) SO_2 sorption isotherms of DMOF and DMOF-X at 293 K between 0 and 0.97 bar.; (b) The enlarged SO_2 adsorption at low-pressure of 0–0.1 bar for better clarity of the onset of steep uptake.; (c) Monte Carlo simulated isotherms of SO_2 adsorption on DMOF and DMOF-X between 0 and 0.4 bar (low-pressure) and 293 K.

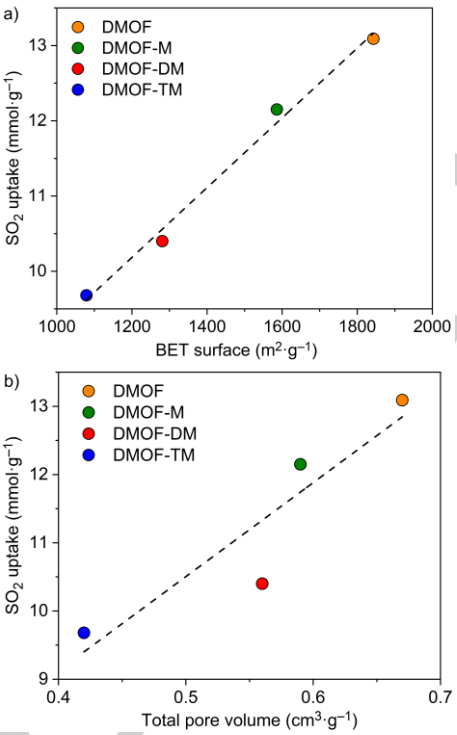

Figure 3. SO_2 uptake (0.97 bar, 293 K) vs (a) BET-surface area and (b) total accessible pore volume (both determined by Ar adsorption at 87 K). The dashed trend lines are a guide to the eye.

The SO_2 adsorption isotherms at 273 and 293 K were used to determine the isosteric enthalpy of SO_2 adsorption ($-\Delta H_{ads}$) by virial analysis (Figure S14-S17, SI).[41] The $-\Delta H_{ads}$ values of methyl-functionalized DMOFs were obviously higher than the parent DMOF and increase with the number of methyl groups (Figure 4). Further, the $-\Delta H_{ads}$ values follow the uptake at low pressure (< 0.05 bar). Grand-canonical-Monte Carlo (GCMC) simulations for a series of small-pore MOFs have shown a good correlation of the SO_2 uptake at reduced pressures (0.05 bar) and the heat of adsorption.[42]

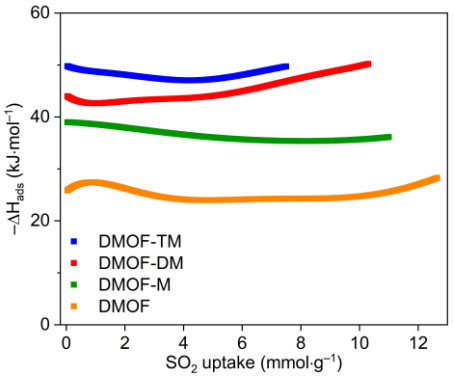

Figure 4. Isosteric enthalpy of adsorption of SO_2 on DMOF and DMOF-X materials from fitting the adsorption isotherms of SO_2 at 273 and 293 K by virial analysis (Figure S14-S17, SI).

At the low pressure of 0.01 bar and 0.1 bar the uptake in the DMOFs is clearly independent of total surface area or pore

10.1002/anie.202105229

volume (Figure 2b). Instead, if the SO_2 uptake at these pressures is normalized by the surface area the surface-specific SO_2 uptake is obtained and can be plotted against the pore limiting diameter (PLD) (Figure 5). The PLD is the smallest diameter of a pore, channel or aperture in a framework. The maximum of surface-specific SO_2 uptake at low-pressure for DMOF-TM at its PLD of ~4.5 Å points to this value as an optimal pore diameter. The value of ~4 Å agrees with the kinetic diameter of SO_2 (4.1 Å).[43] In a pore of width of ~4 Å the SO_2 molecule can have multiple dispersive interactions with the surface. It is obviously an advantage for adsorbent structures to provide Conolly surfaces at a distance of the length of the adsorbed molecule which then can interact at several points with the accessible surface.[44] The Connolly surface is the probe accessible surface.

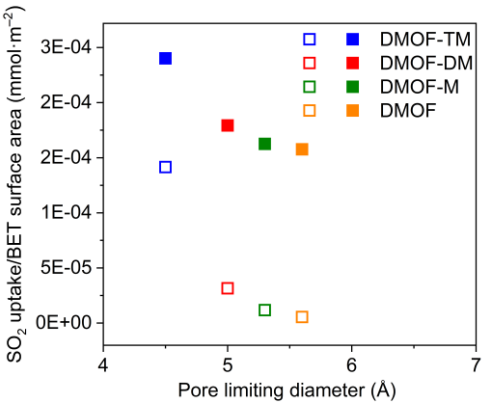

Figure 5. Surface-specific SO_2 uptake at 0.01 bar (open symbols) and 0.1 bar (closed symbols) (293 K), which is the uptake at this pressure divided by the BET-surface area *vs* the pore limiting diameter (PLD). The PLD of DMOF-M and DMOF-DM was determined from their DFT optimized structures (see Section S8.2, Figure S43, SI).

Monte Carlo simulations of SO_2 adsorption at 0-0.4 bar and 293 K were performed on DMOF and DMOF-X using *Cassandra* with standard UFF/UFF4MOF force field parameters.[45] Through the simulated adsorption isotherms the trend of enhanced SO_2 affinity by methyl-functionalized DMOF-X with increased density of methyl groups was well reproduced within the simulations (Figure 2c), despite that the simulated isotherms slightly overestimated the uptake, the most for DMOF-DM (Figure S48, SI). Differences in the simulations occur due to the neglect of structure degradation and possible structure flexibility in the simulations (see the calculation details in the Supporting Information Section S8.2, S9 and Figure S45-46). Also, the choice of force field takes influence on the simulation results (Figure S47 documents the effect of different force fields on the adsorption isotherm of DMOF-TM). Individual parametrization of the host-guest interactions may therefore contribute to further improve the simulation data.

The different SO_2-adsorption behavior of DMOF and DMOF-TM are demonstrated by simulation snapshots at different partial pressures (Figure 6) and by a movie (made with the iRASPA program)[46] showing the consecutive filling with increasing pressure from 0 to 0.4 (40 kPa) (File DMOF2.mp4 in Supp. Info.). In DMOF-TM, it should be noted that SO_2 is preferentially located near the methyl groups of the BDC-TM linkers already at very low pressures, indicating favorable methyl-SO_2 interactions (see below). The pore filling is further enhanced by SO_2-SO_2 dipole-dipole interactions between 0.04 and 0.4 bar. However, SO_2 distribution is sparse in DMOF at the same low-pressure regime (0.01-0.04 bar, Figure 6d, e). The DMOF-SO_2 interactions are weaker (see below) and adsorption is mainly triggered by SO_2-SO_2 dipole-dipole interactions, in which SO_2 molecules prefer to interact with already adsorbed SO_2 molecules (see below). The formation of SO_2 clusters finally fills the pores at 0.4 bar.

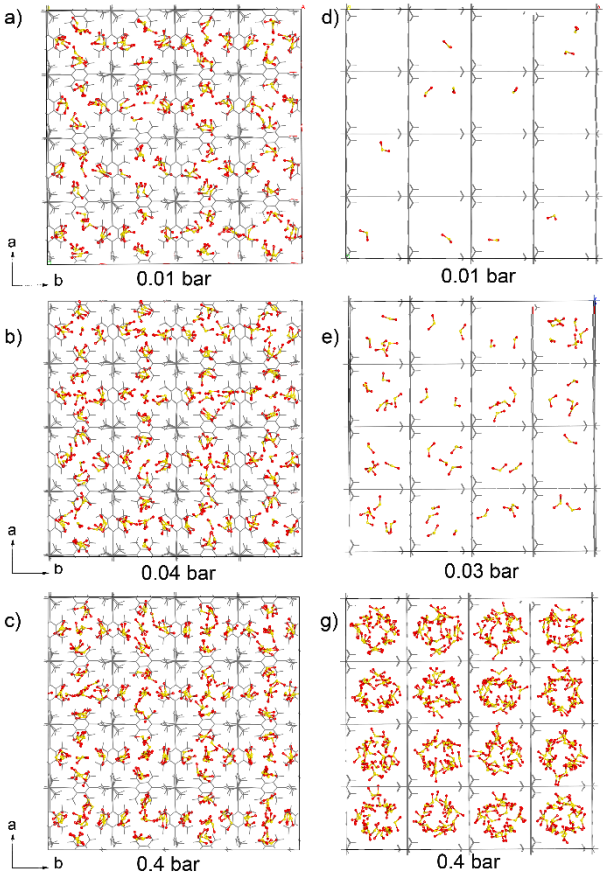

Figure 6. Monte Carlo simulation of SO_2 loading with snapshots at 0.01, 0.03 or 0.04 and 0.4 bar for DMOF-TM (a-c) and DMOF (d-f). See Figure S50, SI for a magnified image and the movie-file DMOF2.mp4, Supp. Info. for the full sequence.

The single-component CO_2, N_2 and CH_4 adsorption isotherms for DMOF and DMOF-X were measured at 293 K (Figure S22-25, SI). The same attribute from the increasing density of methyl groups was also observed with enhanced low-pressure CO_2 and CH_4 adsorption but was not found for N_2 adsorption (Figure S23 and Table S2, SI). However, the increase of low-pressure SO_2 adsorption with methyl density was much steeper than that of CO_2 and CH_4 probably due to the high polarizability (47.7×10^{-25} cm^3) and high dipole moment (1.62 D) of SO_2.[47] At the pressure of 0.97 bar, the uptake of CO_2 and CH_4 increased with the methyl groups density on DMOF-X (Table S2, SI), but the absolute specific amounts of CO_2 and CH_4 were still much lower compared to the SO_2 uptake. The difference in gas uptake, especially at low-pressure, indicates the potential of DMOF-X for selective SO_2 adsorption from flue gases.

In order to evaluate the selectivity of SO_2 over CO_2, CH_4 and N_2 ideal adsorbed solution theory (IAST) calculations were

10.1002/anie.202105229

performed for binary gas mixtures as a function of variable SO_2 molar fractions (from 0.01 to 0.5) at 1 bar and 293 K. Considering the trace SO_2 amount present in the flue gas, high SO_2 selectivity over these other gases is required for a realistic adsorptive gas desulfurization process. For a molar SO_2/CO_2 ratio of 10:90, the selectivity of DMOF was 35, while DMOF-M, -DM and TM afforded the increased selectivity of 38, 40 and 169 (Figure 7 and Table S4, SI). To the best of our knowledge, this SO_2/CO_2 selectivity value of DMOF-TM represents the highest among all MOFs reported so far (Table S4, SI). Meanwhile, DMOF-TM possesses also a high SO_2/CH_4 and SO_2/N_2 selectivity of 725 and 1141, respectively, when the SO_2/CH_4 or SO_2/N_2 ratio is 10:90 (Figure S24-S25, SI).

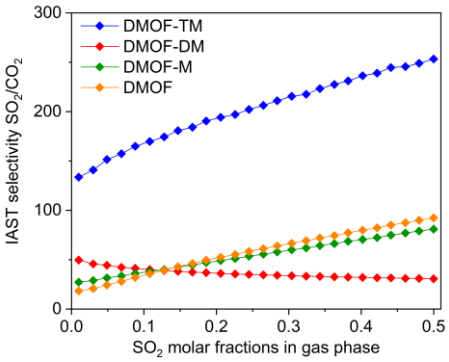

Figure 7. IAST selectivity of SO_2/CO_2 for DMOF-X series as a function of SO_2 molar fractions (0.1-0.5) at 1 bar and 293 K.

The favorable interactions of methyl-functionalized DMOFs with SO_2 over the parent DMOF were elucidated by periodic dispersion-corrected DFT (DFT-D) calculations using *Quantum Espresso*.[48] At least three main binding sites of SO_2 are present within the framework (Figure 8). The adsorbed-SO_2 within the pore surface of DMOF-TM is primarily stabilized by enhanced $(C)H^{(\delta+)}\cdots^{(\delta-)}O(S)$ interactions. The optimized H···O distances of 2.59-2.97 Å between methyl groups and SO_2 are significantly shorter than the sum of vdW radii of H and O atoms (3.05 Å). Multiple $(C)H^{(\delta+)}\cdots^{(\delta-)}O(S)$ interactions between DABCO and SO_2 contribute to structure stabilization with H···O distances of 2.46-2.97 Å (binding site 2 and 3, Figure 8b-c). Furthermore, the optimized (benzene)C··S distances are 3.21-3.38 Å, which are shorter than the analogous value (3.42 Å) in DMOF with SO_2. This indicates the enhanced strength of the $benzene^{(\delta-)}\cdots^{(\delta+)}S$ interactions, which are probably induced by the incorporation of electron-donating methyl groups. The calculated binding energies (–56.9 to –61.0 kJ·mol^{-1}) of SO_2 with DMOF-TM were significantly higher than those (–31.3 to –31.8 kJ·mol^{-1}) with DMOF at the three main binding sites for the first SO_2 molecule (Figure S44, SI). It should be noted that thermal and zero-point energy corrections are not included in this picture. To get an estimate of the zero-point energy contribution, we performed phonon computations for SO_2-bound DMOF-TM (see SI section 8.2), obtaining 8.8 kJ/mol. With this value as a reference, the ZPE-corrected binding energies would range from ca. –48 to –52 kcal/mol. This is in in agreement with the higher experimental $-\Delta H_{ads}$ values of SO_2 on DMOF-TM over DMOF (Figure 4). Subsequently, we explored the effect of increased SO_2 loading on the adsorption of DMOF-TM. DFT-D calculations showed that at least five SO_2 molecules could be trapped within the channel of DMOF-TM (Figure S45-46). Four of them were primarily located in the proximity with BDC-TM linkers *via* noncovalent host-interactions and the other one was adsorbed at the center of the channel *via* SO_2-SO_2 dipole-dipole interactions with other, already adsorbed SO_2 molecules.

Cluster DFT-D calculations were performed with *Gaussian16*[49] to compare the difference in binding interactions between SO_2 and CO_2 on DMOF and DMOF-TM (Figure S41- S42, SI). Similar to periodic DFT-D results, structure optimizations of DMOF-TM with SO_2 yielded multiple non-covalent cooperative interactions (Figure S42, SI). The optimized H···O(S) (2.46-2.81 Å) distances in DMOF-TM models with SO_2 are shorter than those (2.60-2.88 Å) with CO_2. This supports the favorable binding interaction of DMOF-TM with SO_2 over CO_2, in line with the higher binding energies of DMOF-TM with SO_2 (Table S3, SI). Additionally, we performed frequency calculations for the cluster DFT models at the same level of optimization. The resulting adsorption enthalpies for DMOF and DMOF-TM models are in reasonable agreement with the experimental $-\Delta H_{ads}$ values (Table S3).

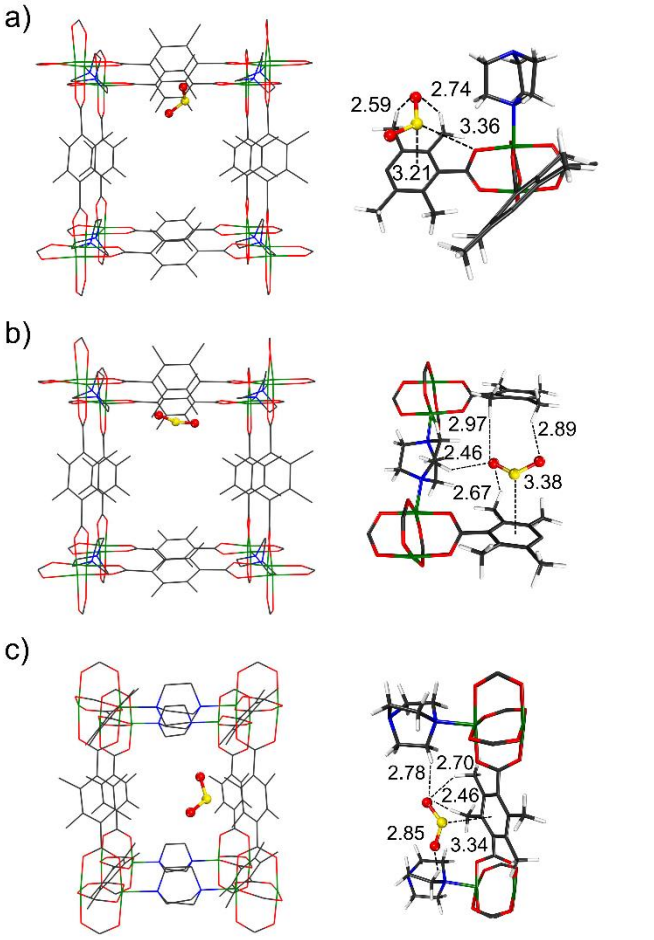

Figure 8. Periodic DFT calculated SO_2 binding sites on optimized DMOF-TM (the distances are given in Å). Binding energy at site 1 (a): –58.0 kJ·mol^{-1}; site 2 (b): –56.9 kJ·mol^{-1}; site 3: –61.0 kJ·mol^{-1}. The respective sites in DMOF are shown in Figure S44, SI. The calculation details are given in Section 8.2, Supporting Information. Color code: S, yellow; O, red; N, blue; Ni, green; C, gray; H, light gray. Hydrogen atoms on framework images in left column are omitted for clarity.

10.1002/anie.202105229

An attempt was made to localize the SO_2 in the pores of the DMOF-TM by powder XRD studies. According to the approximate structural analysis the SO_2 molecules predominantly localize in the largest cavity along the z-axis in the range of x, y, z = 0, 0, 0-0.3 and in the vicinity of two methyl groups of the same Me_4BDC ligand molecule at approximately x, y, z = 0, 0.38, 0.15 (Section S11, SI).

The potential for SO_2 separation from other typical flue gases was investigated by breakthrough experiments and simulations with the ternary gas mixture of $N_2/CO_2/SO_2$ (84.9:15:0.1 v/v/v) at 293 K and 1 bar. From the experimental breakthrough curves (Figure S38 and S39), the immediate rise of N_2 and CO_2 could be clearly seen in both samples of DMOF and DMOF-TM. In contrast, their SO_2 retention time was significantly different. For DMOF-TM (Figure S39), SO_2 can be approximately retained for ~346 min·g^{-1}, but the SO_2 retention time in DMOF (Figure S38) was only ~28 min·g^{-1}. In addition, no significant loss in SO_2 retention time was found in the second and third run of the regenerated DMOF-TM (Figure 9a) with a comparable SO_2 uptake over the three runs (37 *vs* 40 *vs* 37 mg·g^{-1} in the first, second and third run). However, for DMOF (Figure 9b), the total SO_2 loading in the second run was significantly reduced from 5.5 to 3 mg·g^{-1}.

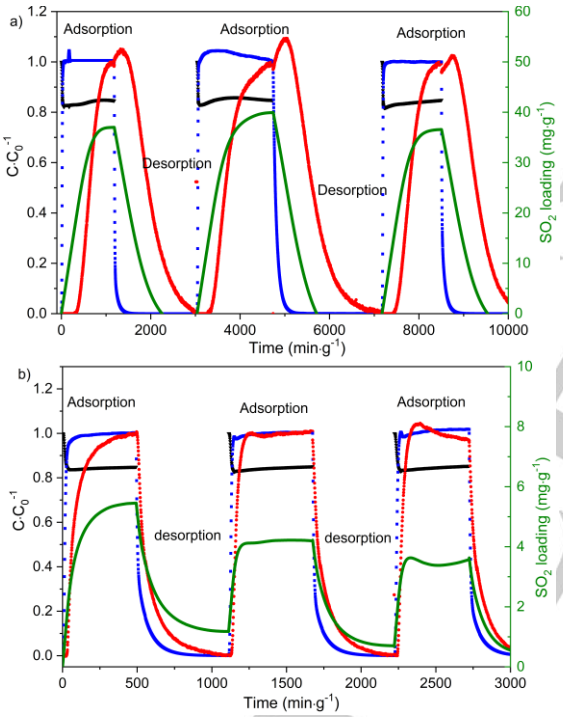

Figure 9. Three runs of adsorption and desorption in cycling breakthrough experiments of DMOF-TM (a) and DMOF (b) sample (red: SO_2; blue: CO_2; black: N_2; green: SO_2 loading uptake; from a ternary gas mixture of $N_2/CO_2/SO_2$ with 84.9:15:0.1 v/v/v at 293 K and 1 bar).

The simulated breakthrough curves have been calculated using the software 3P sim version 1.1.07, employing the "ideal adsorbed solution theory" (IAST) with data from fitted dual-site Langmuir SIPs isotherms.[50] It has been verified that the outcome of the simulations, which were performed using a similar software, matches experimental breakthrough studies, if the separation is based on thermodynamic effects and not on kinetic-steric effects.[51] The breakthrough simulation by the 3P software has already demonstrated to enable a reliable estimate of the breakthrough onset time for SO_2 in gas mixtures.[15,18] From the simulated breakthrough curves, the retention time of SO_2 in the outlet was gradually prolonged by increasing methyl groups on DMOF, in which 6, 14, 63 and 333 min·g^{-1} were recorded for DMOF, DMOF-M, -DM and -TM respectively (Figure S34-37, SI). From the DMOF-TM, the immediate rise of N_2 and CO_2 in the outlet indicates the negligible N_2 and CO_2 adsorption. Thus, the high SO_2/CO_2 and SO_2/N_2 separation performance makes DMOF-TM promising for adsorptive gas desulfurization process.

To investigate the stability of the DMOFs towards SO_2, all activated materials were exposed to dry SO_2 for 6 hours and to humid SO_2 for 6 hours, both at 35 ppm SO_2 content in the air atmosphere (see Section S6, Figure S26, SI). The increasing density of methyl groups did, as expected, gradually improve the structure stability from the evaluation of PXRD patterns and porosity measurements by N_2 sorption. The little changed PXRD patterns of all materials after dry and humid SO_2 exposure suggest the retention of crystallinity without noticeable phase transformation or decomposition (Figure S27, SI). The BET surface area and pore volume on DMOF-DM (~85%) and DMOF-TM (~90%) was also well retained after dry and humid SO_2 (Figure S30-32, SI). DMOF-TM was reported to maintain some crystallinity with a 50% decrease in surface area after 50 ppm SO_2/85% RH/1 day exposure but a complete loss in surface area after 100 ppm SO_2/85% RH/1 day exposure.[25] However, for DMOF (Figure S28, SI), which has no methyl groups, the porosity was significantly reduced under the same SO_2 treatment conditions. For DMOF-M (Figure S29, SI) there was a significant porosity reduction under humid SO_2 exposure.

The regeneration ability of DMOF-TM was further tested by recycling SO_2 adsorption experiment. Considering the $-\Delta H_{ads}$ values of DMOF-TM (~50 kJ·mol^{-1}), we regenerated DMOF-TM by applying vacuum (below 10^{-3} mbar) at room temperature for 1 hour. Remarkably, the SO_2 uptake capacity of re-generated DMOF-TM can be retained for at least four runs of SO_2 adsorption at 0.97 bar and 293 K (Figure S33, SI).

The presence of vibrational modes of remaining adsorbed SO_2 in DMOF-TM under exposure of the SO_2-loaded MOF (see Section S10, SI) to air atmosphere (during 1-20 min) was probed by FT-IR spectra. Two sharp bands at 1331 and 1140 cm^{-1}, not present in pristine DMOF-TM and, hence, associated with the vibrational modes of SO_2 molecules, can be observed in SO_2-adsorbed DMOF-TM (Figure S52). The relative intensity of these bands gradually decreases and the bands have almost disappeared after 20 min. At the same time, several vibrational modes corresponding to the DMOF-TM framework were changed upon SO_2 adsorption (Figure S53): There is (1) a blue-shift of the stretching modes of COO^- (BDC-TM) from 1593 cm^{-1} and 1442 cm^{-1} to 1597 cm^{-1} and 1444 cm^{-1}; (2) a blue-shift of the phenyl bending mode of C=C (benzene of BDC-TM) from 1539 cm^{-1} to 1542 cm^{-1}; (3) a blue-shift of the vibrational mode of -CH_3 (BDC-TM) from 3000 to 3005 cm^{-1} as well as that of -CH_2 (DABCO) from 2943 to 2947 cm^{-1}. These blue-shifted bands, which we attribute to the interactions with the adsorbed SO_2 molecules, are re-established when the SO_2 band have vanished after 20 min.

Conclusion

We have successfully developed a pre-synthetic pore environment tailoring strategy to achieve methyl-functionalized DMOFs with enhanced low-pressure SO_2 adsorption and IAST SO_2/CO_2 selectivity. The improved stability of methyl-

functionalized DMOFs against the highly corrosive SO_2 was attributed to the increased steric hindrance and hydrophobicity induced by increasing density of methyl groups. Benefitting from the tunable pore size and chemistry, DMOF-M and DMOF-DM showed a high SO_2 capacity (12.1 and 10.4 mmol g^{-1}) at 1 bar, while DMOF-TM displayed a high SO_2 uptake at low-pressure (3.79 mmol g^{-1} at 0.01 bar) with a high IAST SO_2/CO_2 selectivity (169, for a molar ratio of SO_2/CO_2 at 10/90). As further demonstrated by the breakthrough simulations, the retention time of SO_2 was the longest on DMOF-TM compared to the other three DMOFs. The exceptionally highly selective SO_2 adsorption on methyl-functionalized DMOFs, especially for DMOF-TM, was attributed to the multiple moderate non-covalent interactions of the small-pore methyl-functionalized framework with SO_2 molecules, as confirmed by DFT calculations. The methyl-design strategy in our work should be also applicable to other isostructural frameworks for highly efficient gas sorption and separations. Also, the expected rotational freedom of the Me_4BDC ligand in DMOF-TM at room temperature might be a factor, which enhances the high affinity to SO_2 as the methyl groups could optimize a double weak-contact with "bridging" SO_2 molecules.

Acknowledgements

S.H. Xing received funding from the Hoffmann Institute of Advanced Materials (HIAM), Shenzhen Polytechnic. The work was supported by the Deutsche Forschungsgemeinschaft (DFG) - 396890929 / GRK 2482. We thank Alex Spieß, Dr. Alexa Schmitz, Daniel Komisarek, Christian Jansen and Dr. Vera Vasylyeva-Shor at Heinrich-Heine-Universität Düsseldorf for help and discussions.

Keywords: Metal-organic frameworks • sulfur dioxide • trace adsorption • separation

[1] X. Han, S. H. Yang, M. Schröder, Porous metal–organic frameworks as emerging sorbents for clean air. *Nat. Rev. Chem.* **2019**, *3*, 108-118.

[2] T. Islamoglu, Z. J. Chen, M. C. Wasson, C. T. Buru, K. O. Kirlikovali, U. Afrin, M. R. Mian, O. K. Farha, Metal–Organic Frameworks against Toxic Chemicals. *Chem. Rev.* **2020**, *120*, 8130-8160.

[3] N. S. Bobbitt, M. L. Mendonca, A. J. Howarth, T. Islamoglu, J. T. Hupp, O. K. Farha, R. Q. Snurr, Metal–organic frameworks for the removal of toxic industrial chemicals and chemical warfare agents. *Chem. Soc. Rev.* **2017**, *46*, 3357-3385.

[4] E. Martinez-Ahumada, A. Lopez-Olvera, V. Jancik, J. E. Sanchez-Bautista, E. Gonzallez-Zamora, V. Martis, D. R. Williams, I. A. Ibarra, MOF Materials for the Capture of Highly Toxic H_2S and SO_2. *Organometallics* **2020**, *39*, 883-915.

[5] Y. Liu, T. M. Bisson, H. Q. Yang, Z. H. Xu, Recent developments in novel sorbents for flue gas clean up. *Fuel Process. Technol.* **2010**, *91*, 1175-1197.

[6] M. A. Hanif, N. Ibrahim, A. Abdul Jalil, Sulfur dioxide removal: An overview of regenerative flue gas desulfurization and factors affecting desulfurization capacity and sorbent regeneration. *Environ. Sci. Pollut. Res.* **2020**, *27*, 27515-27540.

[7] R. K. Srivastava, W. Jozewicz, Flue gas desulfurization: the state of the art. *J. Air Waste Manage. Assoc.* **2011**, *51*, 1676-1688.

[8] L. Zhang, L. Xiao, Y. Zhang, L. J. France, Y. Yu, J. Long, D. Guo, X. Li, Synthesis of Ionic Liquid-SBA-15 Composite Materials and Their Application for SO_2 Capture from Flue Gas. *Energy Fuels* **2018**, *32*, 678−687.

[9] C. Li, D. Lu, C. Wu, Designing tri-branched multiple-site SO_2 capture materials. *Phys. Chem. Chem. Phys.* **2018**, *20*, 16704−16711.

[10] A. Wang, R. Fan, X. Pi, Y. Zhou, G. Chen, W. Chen, Y. Yang, Nitrogen-Doped Microporous Carbon Derived from Pyridine Ligand-Based Metal-Organic Complex as High-Performance SO_2 Adsorption Sorbents. *ACS Appl. Mater. Interfaces* **2018**, *10*, 37407− 37416.

[11] J. B. DeCoste, G. W. Peterson, Metal-organic frameworks for air purification of toxic chemicals. *Chem. Rev.* **2014**, *114*, 5695−5727.

[12] J. Li, Y. Kang, B. Li, X. Wang, D. Li, PEG Linked Functionalized Dicationic Ionic Liquids for Highly Efficient SO_2 Capture through Physical Absorption. *Energy Fuels* **2018**, *32*, 12703−12710.

[13] X. Chen, B. Shen, H. Sun, G. Zhan, Ion-exchange modified zeolites X for selective adsorption desulfurization from Claus tail gas: Experimental and computational investigations. *Microporous Mesoporous Mater.* **2018**, *261*, 227−236.

[14] J. Liang, S. H. Xing, P. Brandt, A. Nuhnen, C. Schlüsener, Y. Y. Sun, C. Janiak, A chemically stable cucurbit[6]uril-based hydrogen-bonded organic framework for potential SO_2/CO_2 separation. *J. Mater. Chem. A* **2020**, *8*, 19799-19804.

[15] J. H. Carter, X. Han, F. Y. Moreau, I. D. Silva, A. Nevin, H. G. W. Godfrey, C. C. Tang, S. H. Yang, M. Schröder, Exceptional Adsorption and Binding of Sulfur Dioxide in a Robust Zirconium-Based Metal−Organic Framework. *J. Am. Chem. Soc.* **2018**, *140*, 15564-15567.

[16] S. H. Yang, L. F. Liu, J. L. Sun, K. M. Thomas, A. J. Davies, M. W. George, A. J. Blake, A. H. Hill, A. N. Fitch, C. C. Tang, M. Schröder, Irreversible Network Transformation in a Dynamic Porous Host Catalyzed by Sulfur Dioxide. *J. Am. Chem. Soc.* **2013**, *135*, 4954-4957.

[17] K. Tan, P. Canepa, Q. H. Gong, J. Liu, D. H. Johnson, A. Dyevoich, P. K. Thallapally, T. Thonhauser, J. Li, Y. J. Chabal, Mechanism of Preferential Adsorption of SO_2 into Two Microporous Paddle Wheel Frameworks $M(bdc)(ted)_{0.5}$. *Chem. Mater.* **2013**, *25*, 4653-4662.

[18] L. Li, I. D. Silva, D. I. Kolokolov, X. Han, J. N. Li, G. Smith, Y. Q. Cheng, L. L. Daemen, C. G. Morris, H. G. W. Godfrey, N. M. Jacques, X. R. Zhang, P. Manuel, M. D. Frogley, C. A. Murray, A. J. Ramirez-Cuesta, G. Cinque, C. C. Tang, A. G. Stepanov, S. H. Yang, M. Schröder, Post-synthetic modulation of the charge distribution in a metal–organic framework for optimal binding of carbon dioxide and sulfur dioxide. *Chem. Sci.* **2019**, *10*, 1472-1482.

[19] L. M. Rodríguez-Albelo, E. López-Maya, S. Hamad, A. R. Ruiz-Salvador, S. Calero, J. A. R. Navarro, Selective Sulfur Dioxide Adsorption on Crystal Defect Sites on an Isoreticular Metal Organic Framework Series. *Nat. Commun.* **2017**, *8*, 14457.

[20] M. Savage, Y. Q. Cheng, T. L. Easun, J. E. Eyley, S. P. Argent, M. R. Warren, W. Lewis, C. Murray, C. C. Tang, M. D. Frogley, G. Cinque, J. L. Sun, S. Rudic, R. T. Murden, M. J. Benham, A. N. Fitch, A. J. Blake, A. J. Ramirez-Cuesta, S. H. Yang, M. Schröder, Selective Adsorption of Sulfur Dioxide in a Robust Metal–Organic Framework Material. *Adv. Mater.* **2016**, *28*, 8705-8711.

[21] J. A. Zarate, E. Sanchez-Gonzalez, D. R. Williams, E. Gonzalez-Zamora, V. Martis, A. Martinez, J. Balmaseda, G. Maurin, I. A. Ibarra, High and energy-efficient reversible SO_2 uptake by a robust Sc(III)-based MOF. *J. Mater. Chem. A* **2019**, *7*, 1558-15584.

[22] H. Furukawa, N. Ko, Y. B. Go, N. Aratani, S. B. Choi, E. Choi, O. Yazaydin, R. Q. Snurr, M. O'Keeffe, J. Kim, O. M. Yaghi, Ultrahigh Porosity in Metal-Organic Frameworks. *Science* **2010**, *329*, 6814-6818.

[23] A. Schoedel, M. Li, M. O'Keeffe, O. M. Yaghi, Structures of Metal-Organic Frameworks with Rod Secondary Building Units. *Chem. Rev.* **2016**, *116*, 12466-12535.

[24] O. M. Yaghi, M. O'Keeffe, N. M. Ockwig, H. K. Chae, M. Eddaoudi, J. Kim, Reticular Synthesis and the Design of New Materials. *Nature* **2003**, *423*, 705-714.

[25] J. Hungerford, S. Bhattacharyya, U. Tumuluri, S. Nair, Z. Wu, K. S. Walton, DMOF-1 as a Representative MOF for SO_2 Adsorption in Both Humid and Dry Conditions. *J. Phys. Chem. C* **2018**, *122*, 23493-23500.

[26] E. Martínez-Ahumada, M. L. Díaz-Ramírez, H. A. Lara-García, D. R. Williams, V. Martis, V. Jancik, E. Lima, I. A. Ibarra, High and reversible SO_2 capture by a chemically stable Cr(iii)-based MOF. *J. Mater. Chem. A*, **2020**, *8*, 11515 -11520.

[27] S. Gorla, M. L. Díaz-Ramírez, N. S. Abeynayake, D. M. Kaphan, D. R. Williams, V. Martis, H. A. Lara-García, B. Donnadieu, N. Lopez, I. A. Ibarra, V. Montiel-Palma, Functionalized NU-1000 with an iridium organometallic fragment: SO_2 capture enhancement. *ACS Appl. Mater. Interfaces* **2020**, *12*, 41758–41764.

[28] E. S. Grape, J. G. Flores, T. Hidalgo, E. Martínez-Ahumada, A. Gutiérrez-Alejandre, A. Hautier, D. R. Williams, M. O'Keeffe, L. Öhrström, T. Willhammar, P. Horcajada, I. A. Ibarra, A. K. Inge, A Robust and Biocompatible Bismuth Ellagate MOF Synthesized Under Green Ambient Conditions. *J. Am. Chem. Soc.* **2020**, *142*, 16795–16804.

[29] K. Tan. S. Zuluaga, H. Wang, P. Canepa, K. Soliman, J. Cure, J. Li, T. Thonhauser, Y. J. Chabal, Interaction of Acid Gases SO_2 and NO_2 with Coordinatively Unsaturated Metal Organic Frameworks: M-MOF-74 (M = Zn, Mg, Ni, Co). *Chem. Mater.* **2017**, *29*, 4227-4235.

[30] G. L. Smith, J. E. Eyley, X. Han, X. Zhang, J. Li, N. M. Jacques, H. G. W. Godfrey, S. P. Argent, L. J. McCormick McPherson, S. J. Teat, Y. Cheng, M. D. Frogley, G. Cinque, S. J. Day, C. C. Tang, T. L. Easun, S. Rudić, A. J. Ramires-Cuesta, S. Yang, M. Schröder, Reversible Coordinative Binding and Separation of Sulfur Dioxide in a Robust Metal-Organic Framework with Open Copper Sites. *Nat. Mater.* **2019**, *18*, 1358–1365.

[31] P. Brandt, A. Nuhnen, M. Lange, J. Möllmer, O. Weingart, C. Janiak, Metal−Organic Frameworks with Potential Application for SO_2 Separation and Flue Gas Desulfurization. *ACS Appl. Mater. Interfaces* **2019**, *11*, 17350-17358.

[32] S. Glomb, D. Woschko, G. Makhloufi, C. Janiak, Metal-Organic Frameworks with Internal Urea-Functionalized Dicarboxylate Linkers for SO_2 and NH_3 Adsorption. *ACS Appl. Mater. Interfaces* **2017**, *9*, 37419-37434.

[33] P. Brandt, A. Nuhnen, S. Öztürk, G. Kurt, J. Liang, C. Janiak, Comparative Evaluation of Different MOF and non-MOF Porous Materials for SO_2 Adsorption and Separation Showing the Importance of Small Pore Diameters for Low-Pressure Uptake; *Adv. Sust. Mater.* **2021**, *5*, 2000285

[34] H. Liu, Y. G. Zhao, Z. J. Zhang, N. Nijem, Y. L. Chabal, H. P. Zeng, J. Li, The Effect of Methyl Functionalization on Microporous Metal-Organic Frameworks' Capacity and Binding Energy for Carbon Dioxide Adsorption. *Adv. Funct. Mater.* **2011**, *21*, 4754–4762.

[35] N. C. Burtch, H. Jasuja, D. Dubbeldam, K. S. Walton, Molecular-level Insight into Unusual Low Pressure CO_2 Affinity in Pillared Metal−Organic Frameworks. *J. Am. Chem. Soc.* **2013**, *135*, 7172−7180.

[36] H. Jasuja, N. C. Burtch, Y. G. Huang, Y. Cai, K. S. Walton, Kinetic Water Stability of an Isostructural Family of Zinc-Based Pillared Metal–Organic Frameworks. *Langmuir* **2013**, *29*, 633–642.

[37] D. N. Dybtsev, H. Chun, K. Kim, Rigid and Flexible: A Highly Porous Metal–Organic Framework with Unusual Guest-Dependent Dynamic Behavior. *Angew. Chem. Int. Ed.* **2004**, *43*, 5033-5036.

[38] P. Maniam, N. Stock, Investigation of Porous Ni-Based Metal-Organic Frameworks Containing Paddle-Wheel Type Inorganic Building Units via High-Throughput Methods. *Inorg. Chem.* **2011**, *50*, 5085-5097.

[39] X. Wang, Z. Niu, A. M. Al-Enizi, A. Nafady, Y. F. Wu, B. Aguila, G. Verma, L. Wojtas, Y. S. Chen, Z. Li, S. Q. Ma, Pore environment engineering in metal–organic frameworks for efficient ethane/ethylene separation. *J. Mater. Chem. A* **2019**, *7*, 13585-13590.

[40] X. L. Cui, L. F. Yang, R. Krishna, Z. G. Zhang, Z. B. Bao, H. Wu, Q. L. Ren, W. Zhou, B. L. Chen, H. B. Xing, Ultrahigh and Selective SO_2 Uptake in Inorganic Anion-Pillared Hybrid Porous Materials. *Adv. Mater.* **2017**, *29*, 1606929.

[41] A. Nuhnen, C. Janiak, A practical guide to calculate the isosteric heat/enthalpy of adsorption via adsorption isotherms in metal-organic frameworks, MOFs. *Dalton Trans.* **2020**, *49*, 10295-10307.

[42] X.-D. Song, S. Wang, C. Hao, J. S. Qiu, Investigation of SO_2 Gas Adsorption in Metal–Organic Frameworks by Molecular Simulation. Inorg. *Chem. Commun.* **2014**, *46*, 277–281.

[43] J.-R. Li, R. J. Kuppler, H.-C. Zhou, Selective Gas Adsorption and Separation in Metal-Organic Frameworks. *Chem. Soc. Rev.* **2009**, *38*, 1477−1504.

[44] M. Thommes, K. Kaneko, A. V. Neimark, J. P. Olivier, F. Rodriguez-Reinoso, J. Rouquerol, K. S. W. Sing, Physisorption of Gases, with Special Reference to the Evaluation of Surface Area and Pore Size Distribution (IUPAC Technical Report). *Pure Appl. Chem.* **2015**, *87*, 1051−1069.

[45] J. K. Shah, E. Marin-Rimoldi, R. G. Mullen, B. P. Keene, S. Khan, A. S. Paluch, N. Rai, L. L. Romanielo, T. W. Rosch, B. Yoo, E. J. Maginn, Cassandra: An open source Monte Carlo package for molecular simulation. *J. Comput. Chem.* **2017**, *38*, 1727–1739.

[46] D. Dubbeldam, S. Calero, T. J. H. Vlugt, iRASPA: GPU-accelerated visualization software for materials scientists. *Molecular Simulation* **2018**, *44*, 653–676.

[47] S. Yang, J. Sun, A. J. Ramirez-Cuesta, S. K. Callear, W. I. F. David, D. P. Anderson, R. Newby, A. J. Blake, J. E. Parker, C. C. Tang, M. Schröder, Selectivity and Direct Visualization of Carbon Dioxide and Sulfur Dioxide in a Decorated Porous Host. *Nat. Chem.* **2012**, *4*, 887–894.

[48] P. Giannozzi, S. Baroni, N. Bonini, M. Calandra, R. Car, C. Cavazzoni, D. Ceresoli, G. L. Chiarotti, M. Cococcioni, I. Dabo, A. Dal Corso, S. de Gironcoli, S. Fabris, G. Fratesi, R. Gebauer, U. Gerstmann, C. Gougoussis, A. Kokalj, M. Lazzeri, L. Martin-Samos, N. Marzari, F. Mauri, R. Mazzarello, S. Paolini, A. Pasquarello, L. Paulatto, C. Sbraccia, S. Scandolo, G. Sclauzero, A. P. Seitsonen, A. Smogunov, P. Umari, R. M. Wentzcovitch, QUANTUM ESPRESSO: A Modular and Open-Source Software Project for Quantum Simulations of Materials. *J. Phys.: Condens. Matter* **2009**, *21*, 1-19.

[49] M. J. Frisch, G. W. Trucks, H. B. Schlegel, G. E. Scuseria, M. A. Robb, J. R. Cheeseman, G. Scalmani, V. Barone, G. A. Petersson, H. Nakatsuji, X. Li, M. Caricato, A. V. Marenich, J. Bloino, B. G. Janesko, R. Gomperts, B. Mennucci, H. P. Hratchian, J. V. Ortiz, A. F. Izmaylov, J. L. Sonnenberg, D. Williams-Young, F. Ding, F. Lipparini, F. Egidi, J. Goings, B. Peng, A. Petrone, T. Henderson, D. Ranasinghe, V. G. Zakrzewski, J. Gao, N. Rega, G. Zheng, W. Liang, M. Hada, M. Ehara, K. Toyota, R. Fukuda, J. Hasegawa, M. Ishida, T. Nakajima, Y. Honda, O. Kitao, H. Nakai, T. Vreven, K. Throssell, J. A., Jr. Montgomery, J. E. Peralta, F. Ogliaro, M. J. Bearpark, J. J. Heyd, E. N. Brothers, K. N. Kudin, V. N. Staroverov, T. A. Keith, R. Kobayashi, J. Normand, K. Raghavachari, A. P. Rendell, J. C. Burant, S. S. Iyengar, J. Tomasi, M. Cossi, J. M. Millam, M. Klene, C. Adamo, R. Cammi, J. W. Ochterski, R. L. Martin, K. Morokuma, O. Farkas, J. B. Foresman, D. J. Fox, Gaussian 16, Revision A.03; Gaussian, Inc., Wallingford CT, **2016**.

[50] A.L. Myers, J. M. Prausnitz, Thermodynamics of Mixed-Gas Adsorption. *AIChE* **1965**, *11*, 121-127.

[51] A. Möller, R. Eschrich, C. Reichenbach, J. Guderian, M. Lange, J. Möllmer, Dynamic and Equilibrium-Based Investigations of CO_2-Removal from CH_4-Rich Gas Mixtures on Microporous Adsorbents. *Adsorption* **2016**, *23*, 197-209.

10.1002/anie.202105229

Entry for the Table of Contents

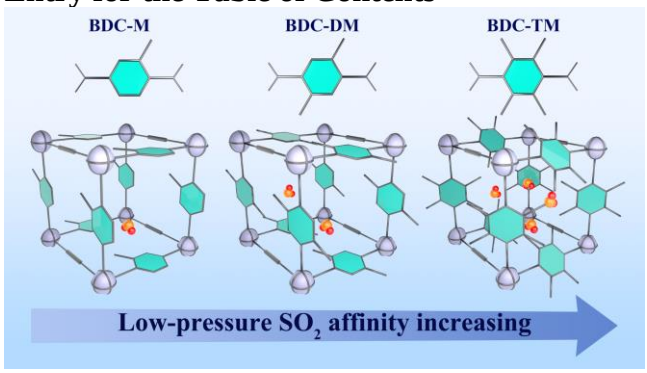

The pre-synthetic pore environment tailoring strategy has been applied to improve low-pressure SO_2 affinity on stable isostructural methyl-functionalized MOFs by controlling methyl groups density. The enhanced low-pressure SO_2 uptake and SO_2 separation was achieved. This work provides a facile strategy to achieve tailor-made MOF adsorbent for challenging gas purification application.

Shanghua Xing, Jun Liang, Philipp Brandt, Felix Schäfer, Alexander Nuhnen, Tobias Heinen, Istvan Boldog, Jens Möllmer, Marcus Lange, Oliver Weingart, and Christoph Janiak**

Page No. – Page No.

Capture and Separation of SO_2 Traces in Metal-Organic Frameworks via Pre-synthetic Pore Environment Tailoring by Methyl Groups